ELSEVIER

Composites Science and Technology 60 (2000) 273–281

COMPOSITES SCIENCE AND TECHNOLOGY

Prediction of impact damage in composite plates

J.P. Hou*, N. Petrinic, C. Ruiz, S.R. Hallett

Department of Engineering Science, Oxford University, Parks Road, Oxford OX1 3PJ, UK

Received 4 February 1999; received in revised form 14 July 1999; accepted 9 August 1999

Abstract

This paper gives details of the implementation of improved failure criteria for laminated composite structures into LS-DYNA3D. Out-of-plane stresses have been taken into consideration for damage initiation. It is suggested, for the first time, that delamination is constrained by through-thickness compression stress. Interactions between different damage mechanisms have been considered. Damage predictions in good agreement with experimental ones have been achieved. © 2000 Elsevier Science Ltd. All rights reserved.

Keywords: B. Impact behaviour; B. Matrix cracking; C. Delamination; C. Failure criterion; C. Finite element analysis

1. Introduction

The Chang–Chang failure criteria [1] and DYNA3D are widely used for the prediction of impact damage in composites [2–5]. Hallett and Symons used the VEC version of the DYNA3D to simulate tension, through-thickness shear and impact tests on beams and plates [6]. The damage processes in beam tension and impact have been successfully modelled by using the material model of composite failure (material 22) [7,8]. That is because the dominant stresses in beam impact were tensile stress in the fibre and transverse directions, i.e. in-plane stresses. Results from the modelling of inter-laminar shear tests on notched specimens showed that stress concentration at the delamination tip introduce a mesh-sensitive effect. Better stress/strain curves were obtained by taking the peak shear stress to be equal to the shear concentration factor multiplied by the mean measured shear strength [9]. In the modelling of plate impact, problems occur with damage prediction, although the force/time history could be simulated reasonably well. It was noticed that delamination occurred before matrix cracking and fibre failure under the impactor site and it was the interface close to the impactor that debonded first and last in the modelling. Experimental observations, however, show that delamination away from free edges can only be induced by other failure modes, such as fibre failure and matrix cracking. Other investigations into the modelling of plate impact by the use of DYNA3D showed similar results [10]. Davies et al. [11] used the Chang–Chang criteria to predict matrix cracking and fibre failure, but for delamination they used a fracture-mechanics-based failure criterion.

Several points concerning the criteria used in the existing DYNA3D code have been noticed. First of all, only plane stresses, such as σ_{11}, σ_{12}, σ_{22}, are considered in the criteria for fibre failure, matrix cracking and matrix crushing. Thus damage prediction may not be satisfactory for some loading cases where out-of-plane stresses are significant. Secondly, interlaminar shear stresses caused by matrix cracking and fibre failure are very important causes of delamination in impact events. Actually, these failures act as stress raisers at the adjacent interface [11]. In the DYNA3D code, related stresses are reduced after failure, and the local stresses close to the damage cannot be modelled realistically. Thus, the interactions between different failure modes are not modelled. Finally, the through-thickness compression stress is taken to have exactly the same effect as the through-thickness tension stress on delamination. In fact compressive stress constrains crack opening. This could be the main reason why delamination occurs before matrix cracking and the interface nearest to the non-impacted face failed last in the plate model which uses the existing DYNA3D.

* Corresponding author. Tel.: +44-1865-273811; fax: +44-1865-273906.

E-mail address: jingping.hou@eng.ox.ac.uk (J.P. Hou).

PII: S0266-3538(99)00126-8

To solve these problems, it is suggested in this paper that delamination is constrained by through-thickness compression. An improved criterion for delamination based on this hypothesis, together with other modified criteria concerning matrix cracking and fibre failure, has been proposed and implemented into LS-DYNA3D Version 940 of the code. The influence of matrix cracking and fibre failure as stress raisers at the adjacent interfaces has been taken into account by reducing the interlamina shear strength.

2. Failure criteria

The composite failure material model of DYNA3D is based on the well-known Chang–Chang failure criteria [1,2], with the delamination criterion proposed by and Brewer and Lagace [12]. These criteria are formulated below. The contribution of the stresses to the failure modes is illustrated in Fig. 1.

2.1. Fibre failure

$$e_f^2 = \left(\frac{\sigma_{11}}{X_T}\right)^2 + \left(\frac{\sigma_{12}}{S_{12}}\right)^2 \geqslant 1 \tag{1}$$

2.2. Matrix cracking

In the case of $\sigma_{22} \leqslant 0$,

$$e_m^2 = \left(\frac{\sigma_{22}}{Y_T}\right)^2 + \left(\frac{\sigma_{12}}{S_{12}}\right)^2 \geqslant 1 \tag{2}$$

2.3. Matrix crushing

In case of $\sigma_{22} < 0$,

$$e_d^2 = \frac{1}{4}\left(\frac{-\sigma_{22}}{S_{12}}\right)^2 + \frac{Y_C^2\sigma_{22}}{4S_{12}^2 Y_C} - \frac{\sigma_{22}}{Y_C} + \left(\frac{\sigma_{12}}{S_{12}}\right)^2 \geqslant 1 \tag{3}$$

2.4. Delamination

$$e_1^2 = \left(\frac{\sigma_{33}}{Z_r}\right)^2 + \left(\frac{\sigma_{23}}{S_{23}}\right)^2 + \left(\frac{\sigma_{31}}{S_{31}}\right)^2 \geqslant 1 \tag{4}$$

where:

σ_{11} - stress in the fibre direction;
σ_{22} - stress in the transverse direction;
σ_{33} - stress in the through-thickness direction;
σ_{12} - shear stress in the plane of fibre and transverse directions;
σ_{23} - shear stress in the plane transverse and through-thickness plane;
σ_{31} - shear stress in the plane of through-thickness and fibre directions;

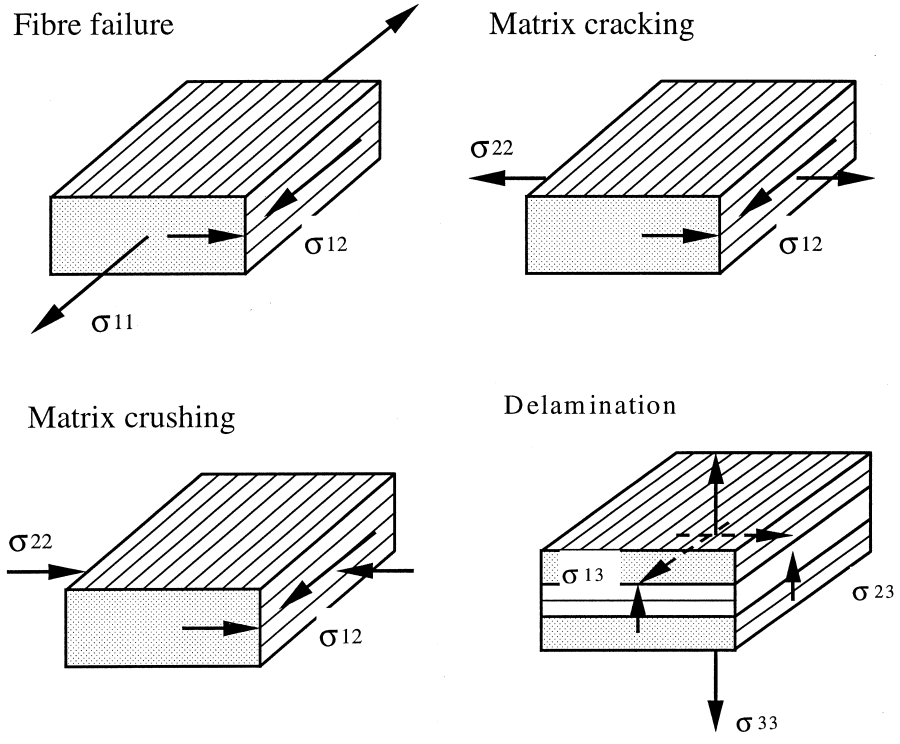

Fig. 1. Stresses inducing failure in DYNA3D failure criteria.

X_T - tensile strength in the fibre direction;
Y_T - tensile strength in the transverse direction;
Y_C - compressive strength in the transverse direction;
Z_T - tensile strength in the through-thickness direction;
S_{12} - shear strength in the fibre and transverse plane;
S_{23} - shear strength in the transverse and through-thickness plane;
S_{31} - shear strength in the through-thickness and fibre plane.

The first three conditions relate to single ply failure and are not unique to the approach but have a great degree of commonality with other widely accepted criteria. Fibre failure may be accepted as governed by Eq. (1), as the tensile stress is the main one that caused fibre failure in blunt head impact. On the other hand, matrix cracking in Eq. (2) does not include the contribution of the shear stress σ_{23}, which is a dominant stress for shear cracking [13,14]. Matrix crushing seldom presents any difficulties in practice in out of plane impact. A serious difficulty on the other hand arises when dealing with delamination, in that the sign of the through-thickness stress σ_{33} is taken to be irrelevant in the criterion currently used in DYNA3D. In reality, compression improves the delamination strength while even small tensile stress by itself can cause delamination. The following modified criteria overcome these difficulties.

2.5. Fibre failure

$$e_f^2 = \left(\frac{\sigma_{11}}{X_T}\right)^2 + \left(\frac{\sigma_{12}^2 + \sigma_{13}^2}{S_f^2}\right) \geqslant 1 \tag{5}$$

2.6. Transverse matrix cracking

In the case of $\sigma_{22} \geqslant 0$

$$e_m^2 = \left(\frac{\sigma_{22}}{Y_T}\right)^2 + \left(\frac{\sigma_{12}}{S_{12}}\right)^2 + \left(\frac{\sigma_{23}}{S_{m23}}\right)^2 \geqslant 1 \tag{6}$$

2.7. Matrix crushing

In the case of $\sigma_{22} < 0$,

$$e_d^2 = \frac{1}{4}\left(\frac{-\sigma_{22}}{S_{12}}\right)^2 + \frac{Y_C^2\sigma_{22}}{4S_{12}^2 Y_C} - \frac{\sigma_{22}}{Y_C} + \left(\frac{\sigma_{12}}{S_{12}}\right)^2 \geqslant 1 \tag{7}$$

2.8. Delamination

In the case of $\sigma_{33} \geqslant 0$,

$$e_l^2 = \left(\frac{\sigma_{33}}{Z_r}\right)^2 + \left(\frac{\sigma_{23}}{S_{l23}}\right)^2 + \left(\frac{\sigma_{31}}{S_{31}}\right)^2 \geqslant 1 \tag{8}$$

where

S_f — shear strength involving fibre failure;
S_{m23} — shear strength for matrix cracking in the transverse and through-thickness plane;
S_{l23} — shear strength for delamination in the transverse and through-thickness plane.

Fig. 2 shows the contribution of each stress to failure modes according to the proposed criteria.

Compared with Eq. (1), in Eq. (5) the shear stress σ_{13} has been taken into account for fibre failure as it has the same effect as the shear stress σ_{12}. It must be pointed out that the shear strength for fibre failure is distinguished from that for matrix cracking, the former should be much higher than the later.

For the criterion of matrix cracking, the contribution of shear stress σ_{23}, which is considered as the cause of shear cracking [13,14], has been included in the new criteria. The criterion for matrix crushing in Eq. (7) remains exactly the same as Eq. (3), as matrix crushing is not the main damage mechanism in impact events.

For delamination, the new criterion has exactly the same form as the existing one in Eq. (4). But delamination is not allowed to occur while an element is under compression in the through-thickness direction. In addition to this, the shear strengths in the transverse and through-thickness plane for matrix cracking and delamination have been separated. There are two reasons for this. Firstly, the shear strength for delamination might be different from that for matrix cracking as there exists a resin rich ply at the interface of plies with different angles which is considered tougher than matrix-fibre interface where high residual thermal stress could be accumulated during processing. The second and the more important reason is that the high shear stresses at the interface induced by fibre failure and matrix cracking are not represented in the model. Instead, the shear stresses are reduced after these failure modes occurred. This means that the model can not give the real interlaminar shear stresses after the presence of these damage modes, which is another difficulty in the prediction of delamination. To cope with this problem, shear strength for delamination in the implemented programme is reduced as a result of interaction of different failure mechanisms.

3. Stress update

Prior to failure, the material is considered as orthotropic linear elastic. The post failure behaviour is modelled following the principles of damage mechanics. Currently, damage parameters are defined as functions of time only, i.e.

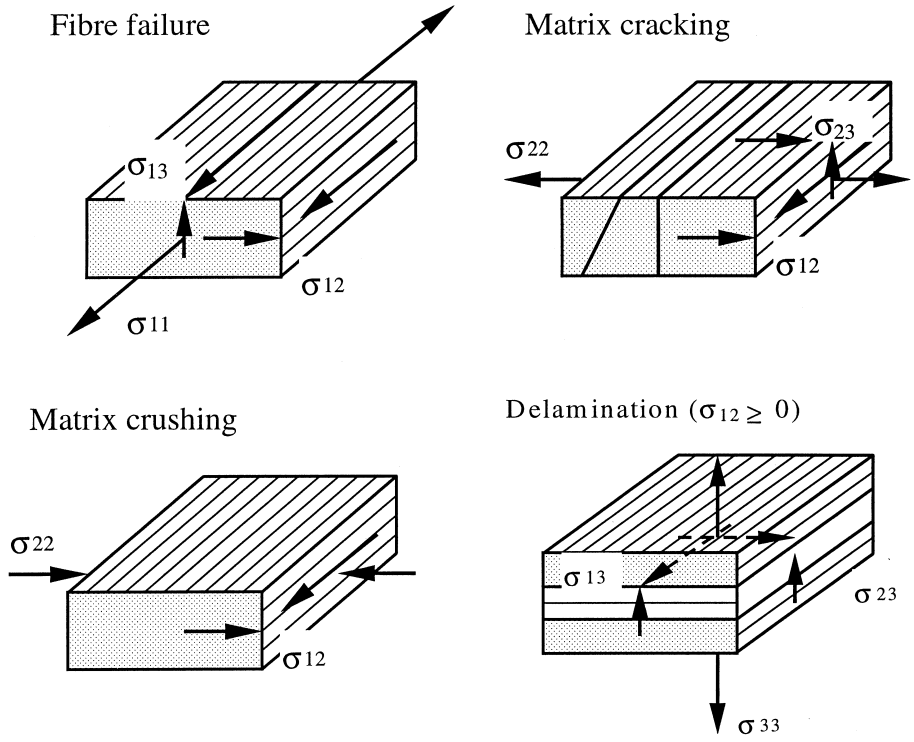

Fig. 2. Stresses inducing failure in the proposed failure criteria.

$$\{d\} = \{d(t)\}\ (0 < d_{ij} < 1) \tag{9}$$

The coupling of damage parameters is illustrated in Table 1, which shows the relation between failure modes and affected components of stress tensor.

Table 1
Damage modes and corresponding stress update

Damage mode	Stresses updated
Fibre failure	$\sigma_{11}=0\ \sigma_{22}=0\ \sigma_{33}=0$ $\sigma_{12}=0\ \sigma_{23}=0\ \sigma_{13}=0$
Matrix cracking	$\sigma_{22}=0\ \sigma_{12}=0$
Matrix crushing	$\sigma_{22}=0$
Delamination	$\sigma_{33}=0\ \sigma_{23}=0\ \sigma_{13}=0$

4. Application to plates under impact

4.1. Experimental work

The new criteria have been implemented into DYNA3D code and used to model the plate impact conducted by Hallett [6,8]. The material tested was unidirectional CFRP T300/914 with a fibre volume fraction of 0.6. The lay-up of the plate were 21 plies of [0°/90°] alternate. The test was carried out using the gas gun shown in Fig. 3. The impactor was a titanium alloy rod 9.55 mm in diameter and 500 mm in length. To ensure the test geometry was the same as those used by the aerospace industry [15,16], the impactor was fitted with a spherically ended steel cap 16 mm in diameter and rubber bungs were used to damp the oscillations in the force signal. The total mass of the impactor was 260 g. In the test, a titanium projectile launched by a gas gun hits the impactor, which then strikes the specimen. The distance between the impactor and the specimen was sufficient to ensure that the former was in a stress-free state on impact. A latch device was fitted so as to avoid multiple impacts when the impactor bounced off the specimen. The dimensions of the plate tested were $85\times85\times2.6$ mm^3. The plate was simply supported by a support block containing a 45 mm diameter circular hole at the centre (as shown in Fig. 4). The velocity of the impactor was measured by infra-red timing gates just before it struck the specimen. C-scan and dye penetrants were used to detect damage after impact.

The damaged plate was sectioned through the centre of the damage region in the direction of the short axis (Table 1). Fig. 5 shows the results of dye penetrant test of plate impacted with an initial velocity of 7.08 ms^{-1}. A delamination-free region was observed just under the impactor, in the through-thickness compression zone under the impactor.

4.2. Numerical modelling

The laminated material was simulated using the failure model defined by the proposed criteria and by the Chang–Chang criteria implemented into the commercially available version of DYNA3D (material 22). The

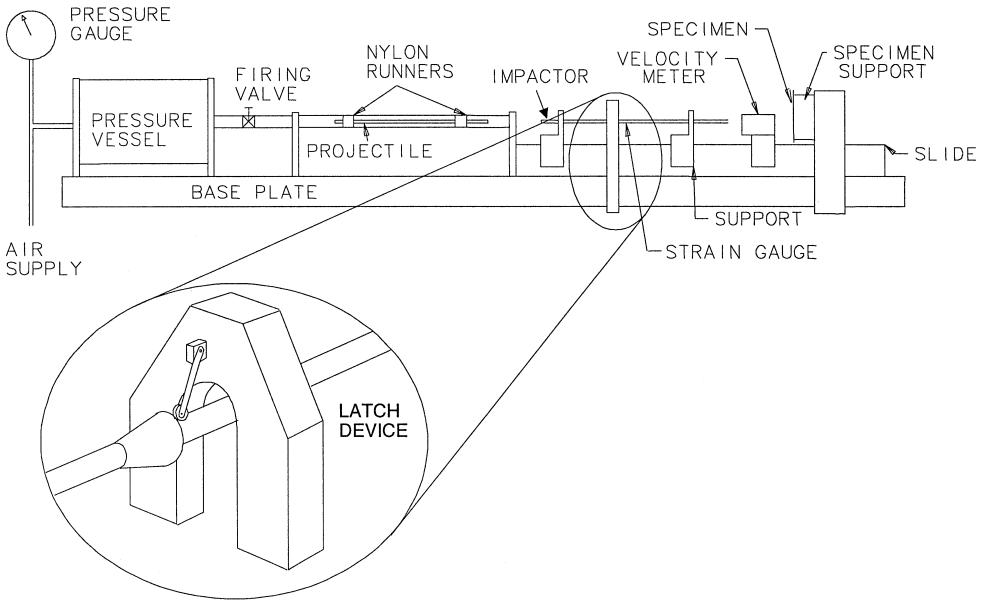

Fig. 3. Set-up of the gas gun apparatus.

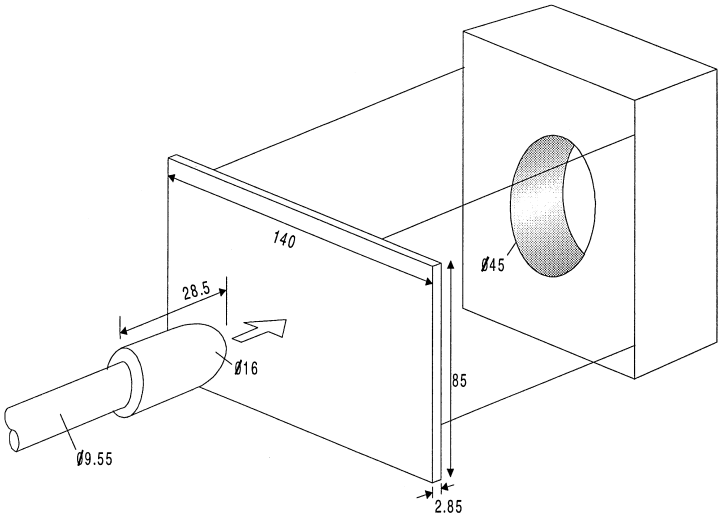

Fig. 4. Support of the plate.

Fig. 5. Dye penetrant test showing delamination of plate impacted at a velocity of 7.08 ms^{-1} (6.5J). The maximum length of delamination is about 19 mm.

model was built based on Hallett's work [8]. The element type is 8-node solid element with one integration point. The laminate was modelled with one element per ply. For simplicity, the impactor was modelled as titanium cylinder of 0.3 m long and 16 mm in diameter with a hemispherical tip, which gives the same mass as that applied in the tests. Elastic isotropic material (material 1 in DYNA3D) was used to simulate the impactor and support materials. Because of symmetry, only one quarter of the structure was modelled in order to save

CPU time. The input material properties are summarised in Table 2. The input file of the model was generated by a pre-processor, PATRAN. D3PLOT was used as post-processor to display the stress, strain, failure situation and other details of the model.

The mesh of the plate model is shown in Fig. 6. A fine mesh was used in the vicinity of the impact zone. The material properties used in the model are shown in Table 2. The support was supplied by a steel ring 45 mm in diameter through surface–surface contact, with the master surface on the ring side. The same type of contact has been applied between the plate and the impactor, which has an initial velocity of 7.08 ms^{-1}. Hourglass control type 5 has been applied to improve the deformation behaviour of elements after failure.

Fig. 7 presents the predicted process of matrix cracking. This starts soon after impact on the compression

Table 2
Material properties applied

Young's modulus in the fibre direction E_1	139E9 (pa)
Young's modulus in the transverse direction E_2	9.4E9 (Pa)
Young's modulus in the normal direction E_3	9.4E9 (Pa)
Poison's ratio ν_{12}	0.0209
Poison's ratio ν_{23}	0.33
Poison's ratio ν_{13}	0.0209
Shear modulus G_{12}	4.5E9 (Pa)
Shear modulus G_{23}	2.98E9 (Pa)
Shear modulus G_{13}	4.5E9 (Pa)
Bulk modulus of failed material K_f	2E9 (Pa)
X_T	2070E6 (Pa)
Y_T	74E6 (Pa)
Y_C	237E6 (Pa)
Z_T	74E6 (Pa)
Shear strength for matrix cracking S_{12}	64E6 (Pa)
Shear strength for matrix cracking S_{m23}	64E6 (Pa)
Shear strength for delamination S_{13}	86e6 (Pa)
Shear strength concerning fibre failure S_f	120E6 (Pa)
Mass density ρ	1.58E3 ($kg.m^{-3}$)

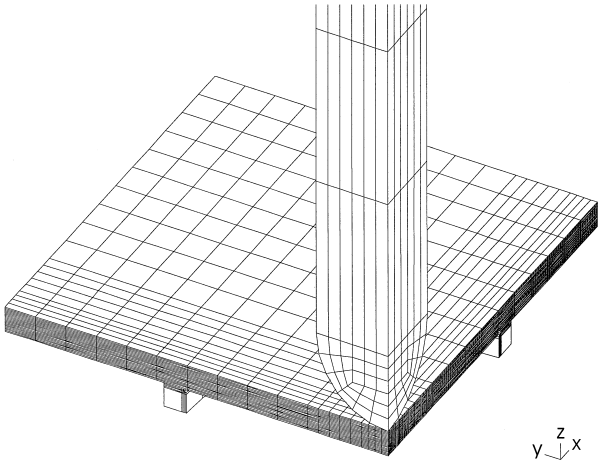

Fig. 6. Mesh of the plate model.

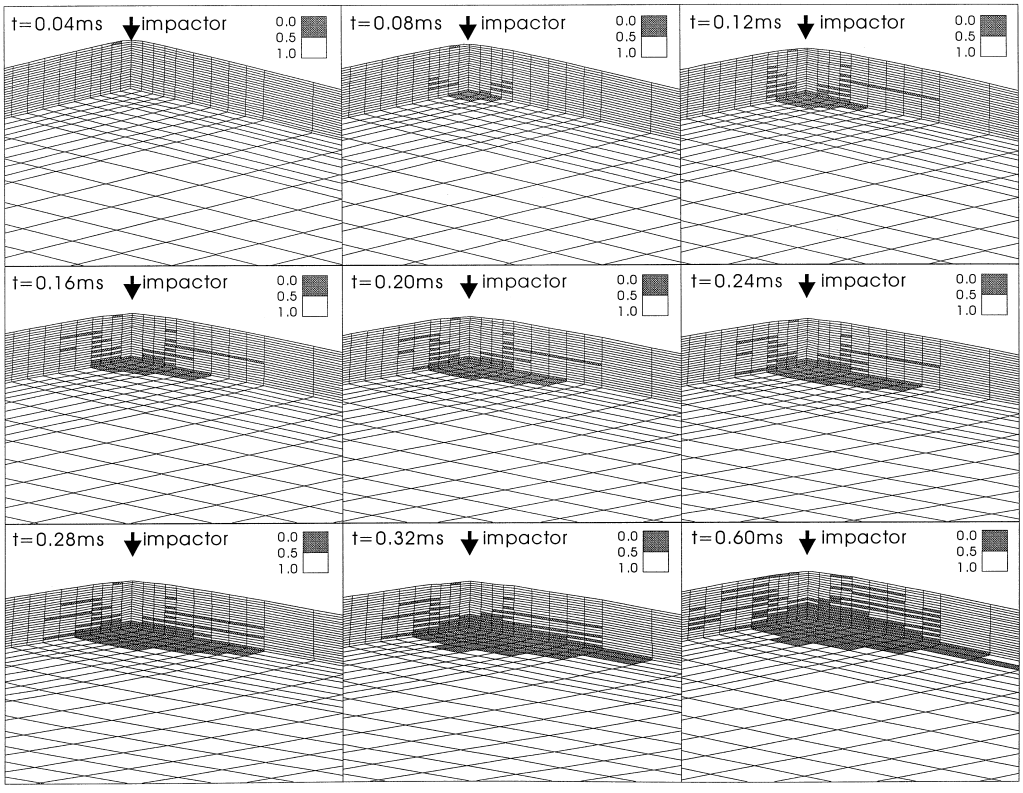

Fig. 7. Predicted matrix cracking from plate model.

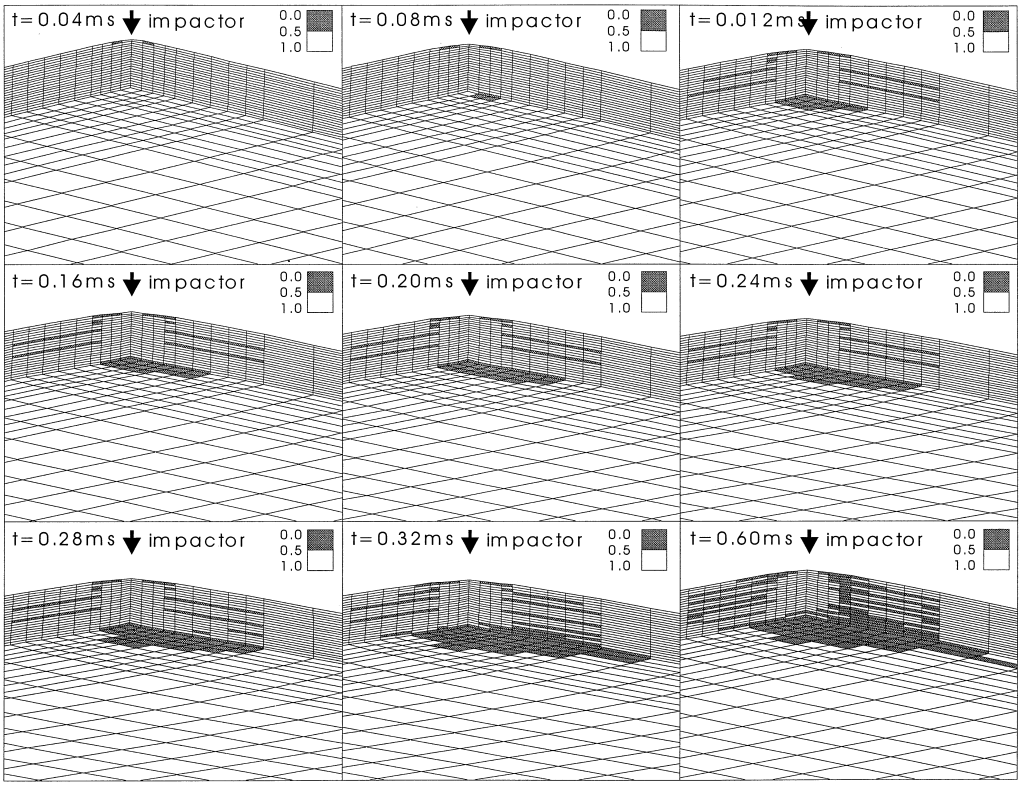

Fig. 8. Predicted delamination from plate model.

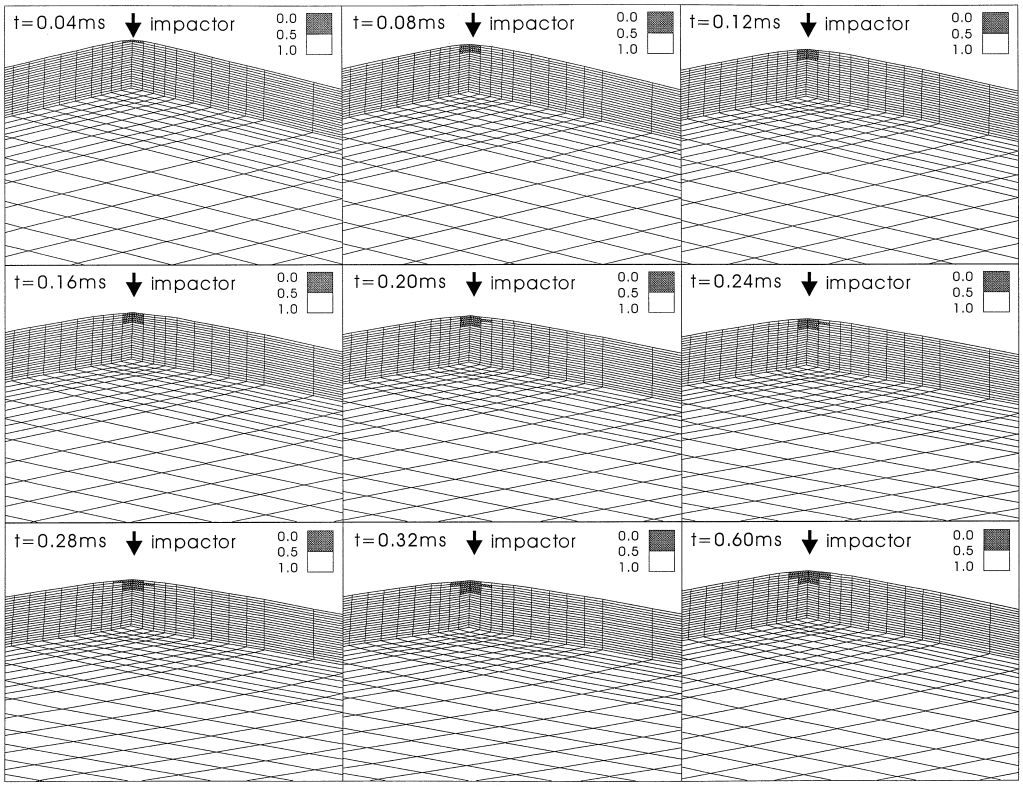

Fig. 9. Predicted matrix crushing from plate model.

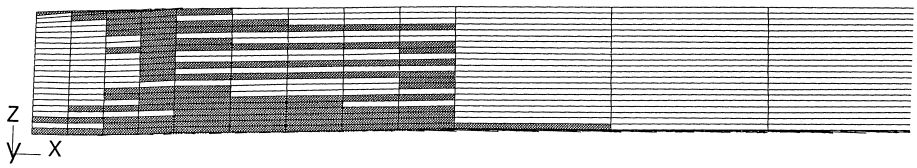

Fig. 10. Predicted delamination after the impactor bounced back ($t = 0.6$ ms).

face, very near to the impactor and is simply caused by the high local compression stress. It will be noted that this limit damage (after 0.04 ms) remains virtually unchanged until much later, at 0.60 ms, by which time extensive matrix cracking has already taken place. For this reason, the initiation of failure for the plate as a whole can be regarded as a totally independent event from the initial matrix cracking. After 0.08 ms, matrix cracking starts in the tension side. This spreads at the same time as laminates nearer to the impacted face begin to crack. However, the main matrix cracking process is related to the extension of cracks in the layers subjected to the maximum tensile stress, i.e. those furthest away from the impact face. Matrix cracking of the internal layers is never very extensive.

Fig. 8 shows the process of delamination. Here again vestigial delamination occurs as a result of Hertzian stress but this extends very little with time. Most of the delamination occurs near the neutral plane of the plate, i.e. between those layers where the maximum shear stress is fond. Delamination progresses rapidly towards the tension side, where it becomes quite extensive, and towards the compression side, where it remains more contained. In comparison with matrix cracking and matrix crushing (Figs. 7 and 9), delamination is seen to present a more severe risk of structural damage. There is, however, a close relationship between matrix cracking and delamination apparent from the two figures. Delamination in the layers in tension is always following the occurrence of matrix cracking there.

Matrix crushing, illustrated in Fig. 9, is never a serious problem since it is always confined to the region immediately in contact with the impactor and results from high Hertzian stress, in good agreement with experimental observations.

In summary, matrix cracking and delamination develop at a very early stage of the contact in the top ply. They are caused by transverse and through-thickness tension stresses induced by Hertzian contact effect, which did not propagate in the thickness direction, except that, matrix cracking in the non-impacted ply initiates at about 65 μm after contact, propagating preferably in the fibre direction of that ply. Shear cracks in the middle plies are some distance away from the impact site, which correspond to experimental observations. Delamination happens at the farthest interface following the matrix cracking, again propagating along the fibre direction as shown in Fig. 8. Delaminations in the inner interfaces are slightly away from the impact site, giving a delamination-free region under the impactor, as found in the experiment.

Fig. 10 shows delamination in the through thickness direction, which is comparable with Fig. 5.

5. Conclusions

Realistic predictions of damage modes, matrix cracking, matrix crushing and delamination have been achieved by the implementation of the improved criteria and the consideration of the interaction of damage modes. Local high shear stresses induced by matrix cracking and fibre failure have been taken into consideration and the interlaminar shear strength was reduced as a result. The delamination-free region just under the impactor observed in impacted plate has been successfully represented by the model. This proves that delamination is constrained by through-thickness compression stress. On the other hand, as the modelled delamination-free region is larger compared with experimental results, it is suggested that delamination should be allowed to happen if the compression stress in the through-thickness direction is relatively small. The interaction between through-thickness compression and shear stresses needs to be studied further.

Acknowledgements

The authors would like to thank the financial support by Rolls Royce Plc.

References

[1] Chang F, Chang K. A progressive damage model for laminated composites containing stress concentrations. Journal of Composite Materials 1987;21:834–55.
[2] Hallquist JO. LS-DYNA3D theoretical manual. Livermore Software Technology Corporation, 1994.
[3] Majeed O, Worswick MJ, Straznicky PV, Poon C. Numerical modelling of transverse impact on composite coupons. Canadian Aeronautics and Space Journal 1994;40(3):99–106.
[4] Edlund A. Finite element modelling of low velocity impact damage in composite laminates. In: Proc ICCM 9, Madrid, July 1993. p. 334–41.
[5] Murray Y, Schwer L. Implementation and verification of fibre composite damage models. NASA Technical Report AD-A216600, December 1989.

[6] Hallett SR, Symons DD. Testing and modelling of impact failure mechanism in carbon fibre. In: Proc NAFEMS World Congress, Stuttgart, April 1997. p. 1232–41.
[7] Symons DD. Impact damage tolerance of carbon fibre reinforced plastics. D. Phl thesis, Oxford University, 1997.
[8] Hallett SR. Small specimen impact testing and modelling of carbon fibre T300/914. D. Phl thesis, Oxford University, 1997.
[9] Hallett SR, Ruiz C, Harding J. The effect of strain rate on the interlamina shear strength of a carbon/epoxy cross ply laminate: comparison between experimental and numerical prediction. Composites Science and Technology, 1999;59:748–58.
[10] Hou JP. Modelling of low velocity impact of beam and plates. UTC Report No.119, April 1998.
[11] Davies AGO, Zhang X, Hitchings D. Modelling impact damage in laminated composites. In: Proc. NAFEMS World Congress, Stuttgart, April 1997. p. 1216–31.
[12] Brewer JC, Lagace PA. Quadratic stress criterion for initiation of delamination. Journal of Composite Materials 1988;22(12):1141–55.
[13] Hyung YC, Downs RJ, Chang FK. A new approach toward understanding damage mechanisms and mechanics of laminated composites due to low-velocity impact: part I — experimental. Journal of Composite Materials 1991;25(8):992–1011.
[14] Hyung YC, Downs RJ, Chang FK. A new approach toward understanding damage mechanisms and mechanics of laminated composites due to low-velocity impact: part II — analysis. Journal of Composite Materials 1991;25(8):1012–38.
[15] Airbus Industrie, Fibre reinforced plastics-determination of compression strength after impact. Airbus Industrie Test Method 1.0010, 1993, Issue 1, February.
[16] Boeing, Advanced composite tests. Boeing Specification Support Standard, BSS7260, Rev C, 1998.